



**HAL**  
open science

## External Laminar Boundary Layer Simulations Using a High-Fidelity Wall-Modeling Approach

Eron Tiago Viana Dauricio, Carlos Junqueira Junior, Diego Ferolla de Abreu,  
João Luiz F. Azevedo

► **To cite this version:**

Eron Tiago Viana Dauricio, Carlos Junqueira Junior, Diego Ferolla de Abreu, João Luiz F. Azevedo. External Laminar Boundary Layer Simulations Using a High-Fidelity Wall-Modeling Approach. Proceedings of the 19th Brazilian Congress of Thermal Sciences and Engineering 2022, Nov 2022, Bento Gonçalves, Brazil. hal-04071994

**HAL Id: hal-04071994**

**<https://hal.science/hal-04071994>**

Submitted on 17 Apr 2023

**HAL** is a multi-disciplinary open access archive for the deposit and dissemination of scientific research documents, whether they are published or not. The documents may come from teaching and research institutions in France or abroad, or from public or private research centers.

L'archive ouverte pluridisciplinaire **HAL**, est destinée au dépôt et à la diffusion de documents scientifiques de niveau recherche, publiés ou non, émanant des établissements d'enseignement et de recherche français ou étrangers, des laboratoires publics ou privés.

# EXTERNAL LAMINAR BOUNDARY LAYER SIMULATIONS USING A HIGH-FIDELITY WALL-MODELING APPROACH

## Eron T. V. Dauricio

Instituto Tecnológico de Aeronáutica, 12228-900, São José dos Campos, SP, Brazil  
eron.tiago90@gmail.com

## Carlos Junqueira-Junior

Arts et Métiers Institute of Technology, DynFluid, CNAM, HESAM University, 151 Boulevard de l'Hôpital, 75013, Paris, France  
junior.junqueira@ensam.eu

## Diego F. Abreu

Instituto Tecnológico de Aeronáutica, 12228-900, São José dos Campos, SP, Brazil  
mecabreu@yahoo.com.br

## João Luiz F. Azevedo

Instituto de Aeronáutica e Espaço, 12228-904, São José dos Campos, SP, Brazil  
joaoluiz.azevedo@gmail.com

**Abstract.** *Wall-Modeled Large Eddy Simulation (WMLES) is a well-established technique for obtaining high-fidelity solutions of turbulent, high Reynolds number flows, with reasonably acceptable computational costs. However, for external flows, the very thin laminar boundary layer developing near the body leading edge imposes quite restrictive mesh resolution requirements, leading to prohibitively high computational costs for practical Reynolds numbers. We propose a wall-modeling approach for the laminar portion of the boundary layer in order to alleviate these costs by reducing the aforementioned mesh resolution requirements. The wall model is based on local self-similar solutions of the boundary layer, and is implemented in the same context of wall-stress models in the WMLES approach. An assessment of the model is done in terms of both pressure and skin friction coefficient distributions along the surface, for an incompressible, fully laminar flow around a NACA 0012 airfoil geometry, with a chord Reynolds number of  $Re_c = 4.5 \times 10^3$ . The results obtained in the simulations using the proposed model are in good agreement with the reference solution, demonstrating the feasibility of the model for external laminar flows.*

**Keywords:** *Wall-Modeling, Wall-Modeled Large Eddy Simulation, External Laminar Flow, Boundary Layer Flow*

## 1. INTRODUCTION

Large Eddy Simulations (LES) have now greatly superseded the long-standing Reynolds-Averaged Navier-Stokes (RANS) approach as a research tool for the study of turbulent flow dynamics in academic and research centers, primarily due to the higher accuracy and fidelity of the resulting simulations. The higher accuracy and resolution of the former is achieved by directly resolving the energetic scales of the turbulent motions, whereas in the latter, all the turbulent motions are modeled. As a consequence, the computational cost of the LES approach is much greater than that of RANS, becoming prohibitively high for practical engineering configurations and high Reynolds number flows.

In the LES approach, only the larger, energy-containing scales are resolved, while the effects of the smaller ones are modeled. However, near the wall, where the boundary layer develops and the turbulent scales are very small, proportional to the viscous length,  $\delta_\nu$ , there is a peak in turbulent energy production (Pope, 2000; Schiavo *et al.*, 2017) that must be captured by the LES simulation. Since the smallest scales become smaller as the Reynolds number increases, the computational cost of resolving for the near-wall region becomes prohibitive for high Reynolds number flows. This situation configures the so-called “LES near-wall problem”.

During the past few decades, many different solutions have been proposed to tackle the LES near-wall problem, all of which incorporates some way of modeling the effects of the near-wall motions onto the overall turbulent flow,

instead of directly resolving it. Among such modeling propositions are the Detached-Eddy Simulation (DES) approach, hybrid RANS/LES approach and wall-stress modeled LES (Deardorff, 1970; Schumann, 1975; Piomelli and Balaras, 2002; Spalart, 2009). These methods are all considered forms of the Wall-Modeled Large Eddy Simulation (WMLES) approach, as opposed to the traditional Wall-Resolved Large Eddy Simulation (WRLES).

Earlier estimates of grid point requirements (Choi and Moin, 2012) show that, for the WMLES approach, a scaling of  $N_{wm} \propto Re_L$  is achieved, compared to  $N_{wr} \propto Re_L^{13/7}$  and  $N_{DNS} \propto Re_L^{37/14}$  for WRLES and DNS computations, respectively. In addition, methods within the WMLES approach break the scaling of computational cost with  $Re_\tau$ , the Reynolds number based on the friction velocity,  $u_\tau = \sqrt{\tau_w/\rho}$ , since in these methods the inner layer is completely modeled, and the cost of resolving the outer layer is independent of  $Re_\tau$  (Larsson *et al.*, 2016). Therefore, the WMLES approach have the potential of achieving high fidelity, high accuracy results, with a much lower computational cost, making such simulations feasible for high Reynolds number flows.

As promising as the WMLES approach may be, there are still some challenges to be faced. One problem with the method that has attracted some attention only recently is the cost of accurately resolving the complete boundary layer in external flows. The current common practice is to employ some form of tripping in the body leading edge to force the boundary layer to be fully turbulent along the surface. However, if WMLES is to be used in contexts other than turbulent research, such as in the engineering design process, then, it is paramount that the developing laminar boundary layer is also accurately resolved, including the region where transition to turbulence occurs.

Larsson *et al.* (2016) estimated the cost of resolving the boundary layer flow along the surface of a NACA0012 airfoil. Even if the WMLES is employed, meaning that only the outer boundary layer is resolved, the number of grid points is massive near the leading edge, where the developing laminar boundary layer is very thin, being proportional to  $1/\delta^2(x)$ . In another study, it has been estimated that the cost of accurately solving the very thin laminar boundary layer near the leading edge of an airfoil may be 10 to 100 times higher than the cost of solving the modeled turbulent region (Slotnick *et al.*, 2014). These estimates show that, for high Reynolds number external flows, even the WMLES is still unfeasible due to high computational costs.

In this work, we propose a wall-modeling strategy for the laminar region of the boundary layer in order to alleviate the computational cost of accurately solving the thin boundary layer near the body leading edge in external flows. The laminar modeling procedure described in this work is applied in the same way as wall-stress models in the WMLES approach, since these are intended to be combined as seamlessly as possible into a single, complete flow simulation process.

## 2. NUMERICAL METHODOLOGY

### 2.1 Governing Equations

The governing equations to be solved numerically are the compressible Navier-Stokes equations, which may be written in conservation form and compact vector notation as

$$\frac{\partial \mathbf{Q}}{\partial t} + \nabla \cdot \mathbf{F}(\mathbf{Q}, \nabla \mathbf{Q}) = 0 \quad (1)$$

where  $\mathbf{Q} = [\rho, \rho u_i, \rho E]^T$  is the vector of conserved variables, and  $\mathbf{F}$  is the flux vector, given by  $\mathbf{F} = \mathbf{F}^e - \mathbf{F}^v$ , with the superscripts  $e$  and  $v$  indicating advective, or Euler, and viscous fluxes, respectively. These may be further written as

$$\mathbf{F}_i^e = \begin{bmatrix} \rho u_i \\ \rho u_1 u_i + \delta_{1i} p \\ \rho u_2 u_i + \delta_{2i} p \\ \rho u_3 u_i + \delta_{3i} p \\ (\rho E + p) u_i \end{bmatrix}, \quad \mathbf{F}_i^v = \begin{bmatrix} 0 \\ \tau_{1i} \\ \tau_{2i} \\ \tau_{3i} \\ u_j \tau_{ij} - q_i \end{bmatrix}, \quad i = 1, 2, 3 \quad (2)$$

In the above equations,  $\rho$  is the density,  $u_i$  are the components of the velocity vector, and  $\rho E$  is the total energy per unit volume. In order to obtain closure of the system of equations, the total energy per unit volume is written in terms of the thermodynamic pressure using the thermal and caloric equations of state for an ideal gas, that is,  $p = \rho R T$  and  $e = c_v T$ , respectively. Then, one can write

$$\rho E = \rho e + \frac{1}{2} \rho u_i u_i = \frac{p}{(\gamma - 1)} + \frac{1}{2} \rho u_i u_i$$

where  $e$  is the internal energy per unit mass, and  $\gamma$  and  $R$  are the ratio and the difference between specific heats, respectively.

The viscous stress tensor,  $\tau_{ij}$ , may be written as

$$\tau_{ij} = \mu \left( \frac{\partial u_i}{\partial x_j} + \frac{\partial u_j}{\partial x_i} \right) + \lambda \left( \frac{\partial u_k}{\partial x_k} \right) \delta_{ij} \quad (3)$$

where  $\mu$  and  $\lambda$  are the dynamic and the second coefficients of viscosity, related by Stokes' hypothesis as  $\lambda = -\frac{2}{3}\mu$ . The heat flux vector,  $q_i$ , in Eq. (2) is given by

$$q_i = -k \frac{\partial T}{\partial x_i}$$

with  $k$  as the thermal conductivity coefficient.

## 2.2 Numerical Method

In this work, Eq. (1) is numerically solved through a nodal implementation of the discontinuous Galerkin (DG) scheme with split formulations for the inviscid fluxes. We start by discretizing the physical domain,  $\Omega$ , into  $K$  non-overlapping elements,  $\Omega_k$ , such that

$$\Omega \approx \Omega_h \equiv \bigcup_{k=1}^K \Omega_k, \quad \bigcap_{k=1}^K \Omega_k = \emptyset$$

where  $\Omega_h$  is the computational domain.

The elements in physical domain are then mapped onto a standard element,  $\Omega_{st}$ , where each shape in physical domain have a corresponding shape in the standard domain. Although the shape of the discretizing elements are arbitrary, in this work we use only hexahedral elements, primarily due to computational efficiency and ease of implementation. For this shape, the standard element is defined by  $\Omega_{st} = [-1, 1]^3$ . Applying this mapping to Eq. (1) results in

$$\mathbf{J} \frac{\partial \mathbf{Q}}{\partial t} + \nabla_{\xi} \cdot \mathcal{F} \equiv \mathbf{J} \frac{\partial \mathbf{Q}}{\partial t} + \nabla_{\xi} \cdot (\mathbf{e}^{\xi} \cdot \mathbf{F}) = 0 \quad (4)$$

where  $\nabla_{\xi}$  is the divergence with respect to the standard element coordinates,  $\xi = (\xi, \eta, \zeta)$ ,  $\mathbf{J} = |\partial \mathbf{x} / \partial \xi|$  is the Jacobian of the coordinate transformation,  $\mathbf{e}^{\xi}$  is the contravariant basis vector, and  $\mathcal{F} = \mathbf{e}^{\xi} \cdot \mathbf{F}$  the contravariant flux vector.

For the nodal implementation of the discontinuous Galerkin scheme, the solution within each element, in standard coordinates, is approximated by a polynomial interpolation given by

$$\mathbf{Q} \approx \mathbf{Q}_h(\xi) = \sum_{p,q,r=0}^N \mathbf{Q}_h(\xi_p, \eta_q, \zeta_r, t) \phi_{pqr}(\xi) \quad (5)$$

where  $\phi_{pqr}$  is the interpolating polynomial. For hexahedral elements, this polynomial is given by a tensor product of 1-D Lagrange polynomials, that is,

$$\phi_{pqr}(\xi) = \ell_p(\xi) \ell_q(\eta) \ell_r(\zeta), \quad \ell_p = \prod_{\substack{i=0 \\ i \neq p}}^{N_p} \frac{\xi - \xi_i}{\xi_p - \xi_i}$$

with equivalent definitions for the other directions.

In the DG formulation, the residual of the approximation, obtained by substitution of Eq. (5) into Eq. (4), is required to be orthogonal to a test function,  $\psi$ , where the space of this test function is the same as the space spanned by the trial, or solution function. This leads to the following formulation

$$\int_{\Omega_{st}} \mathbf{J} \frac{\partial \mathbf{Q}_h}{\partial t} \psi d\xi + \int_{\Omega_{st}} (\nabla_{\xi} \cdot \mathcal{F}^e) \psi d\xi + \int_{\partial \Omega_{st}} (\mathcal{F}^{e,*} - \mathcal{F}^e) \psi d\mathbf{S}_{\xi} - \int_{\Omega_{st}} (\nabla_{\xi} \cdot \mathcal{F}^v) \psi d\xi = 0, \quad (6)$$

where  $\partial \Omega_{st}$  defines the boundary of the element, and  $\mathcal{F}^{e,*}$  is a numerical flux function defined on this boundary. The formulation in Eq. (6) is obtained after integration by parts of the second term of Eq. (4) two times, and is called the strong formulation. The weak formulation is obtained when integration by parts is done only once. The integrals in Eq. (6) are carried out through Gaussian quadratures, where the details may be consulted in Hindenlang *et al.* (2012).

As mentioned above, a split formulation of the inviscid fluxes,  $\mathcal{F}^e$ , is implemented in order to enhance stability of the method, especially for higher order interpolations. The details of this formulation are not described here due to brevity, but may be consulted in the comprehensive exposition of Gassner *et al.* (2016). The specific split form of the fluxes employed throughout the simulations in this work is that of Pirozzoli (2011). An approximate Riemann solver, namely the Roe solver with an entropy fix (Toro, 2009), is used to obtain the numerical flux  $\mathcal{F}^{e,*}$  on the element boundaries.

Since weak variational formulations using discontinuous function spaces are not suitable for directly discretizing higher order derivatives, as those appearing in the divergence term of the viscous fluxes in Eq. (4) through the viscous

stress tensor, Eq. (3), a mixed formulation must be used for these terms. In this work, we make use of the lifting scheme of Bassi and Rebay (2000).

The semidiscrete equations obtained after full discretization of Eq. (6) according to the aforementioned methods are advanced in time using the five stage, fourth-order, low-storage Runge-Kutta scheme of Carpenter and Kennedy (1994). This work uses the computational implementation of the FLEXI software (Krais *et al.*, 2021) in order to apply the numerical scheme and discretization methods just described.

### 3. WALL-STRESS MODELING

#### 3.1 Wall-Modeling Framework

This section briefly outlines the wall-modeling procedure employed in wall-stress models for LES computations, since the laminar wall model proposed in this work is implemented within this same context. For a comprehensive exposition and further details, the reader is referred to previous reviews, *e.g.*, Larsson *et al.* (2016) and Piomelli and Balaras (2002).

The main idea of the WMLES approach is to model the inner part of the boundary layer, which scales with the viscous length,  $\delta_v = \nu/u_\tau$ , and directly resolve only the outer layer, which scales with the boundary layer thickness,  $\delta$ . In doing so, grid requirements near the wall are greatly relaxed, reducing the computational cost by a great amount, as mentioned in previous sections. Moreover, as the dynamics of the inner layer is under-resolved, the approach further reduces the computational cost by reducing the temporal stiffness induced by the viscous sublayer, meaning that larger time-step sizes may be used (Bose and Park, 2018).

The effects of the inner layer onto the overall boundary layer dynamics are accounted for by prescribing the wall-shear stress,  $\tau_w$ , as a boundary condition. From a numerical and mathematical point of view, the approach basically replaces a Dirichlet boundary condition on velocity, where the no-slip condition states that  $\mathbf{u}_w = 0$ , by a Neumann-type boundary condition on the velocity gradients through the computed wall-shear stress – see Eq. (3).

Although the peak turbulence production in the inner layer is not captured by this approach, it is still physically consistent with the fact that, in high Reynolds number flows, the Reynolds stresses are predominantly produced at the same wall distance as they are later dissipated (Hoyas and Jiménez, 2006) and, hence, the method is actually resolving the majority of the boundary layer turbulence production and dissipation. The WMLES approach is also consistent with Townsend’s similarity hypothesis, which states that the shear stresses and the no-transpiration conditions at the wall are sufficient to define the outer flow of the boundary layer (Larsson *et al.*, 2016).

In the context of wall-stress models, in order to calculate a wall-shear stress for boundary condition imposition, the LES solution at a distance  $h_{wm}$  away from the wall in the normal direction is used as the input for a wall model, which, in turn, computes a wall-shear stress and provides this information back to the LES simulation. This process is illustrated in Fig. 1. The distance from the wall where the LES solution is taken is termed the wall-model height or, similarly, the exchange location, where information between the wall model and the LES solution is exchanged. Note that the mesh may be unstructured, with arbitrary shape elements near the wall, and a structured-like grid is shown in Fig. 1 only for simplicity.

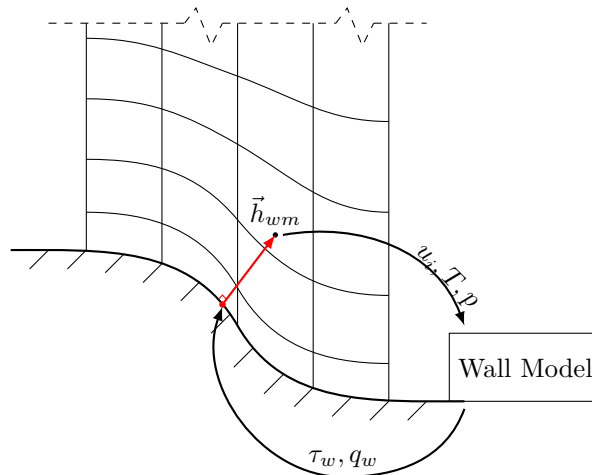


Figure 1: Schematic representation of the wall-modeling procedure employed in the context of WMLES, also used in this work.

The information taken from the LES solution is usually the velocity field,  $\mathbf{u}$ , but may be any other relevant quantity, such as pressure gradients, temperature, and more. If the energy equation is part of the dynamical system being solved, then the imposed boundary condition is augmented with the heat flux,  $q_w$ , which is also computed by the model. It should

be noted that in this wall-modeling methodology, the velocity at the wall is allowed to slip in the wall-tangent direction, and only the no-transpiration condition is used, where the velocity component normal to the wall vanishes.

Throughout the decades, many wall models have been proposed, from simple algebraic models to more complex, PDE-based ones (Bose and Park, 2018). The models included in the latter category make use of the thin boundary layer equations (TBLE), where a PDE must be solved in the region near the wall in order to compute a wall-shear stress. Such models are very general, with only mild underlying assumptions, but are usually difficult to implement. On the other hand, algebraic models have a straightforward implementation, but lacks generality, where it is usually assumed that the boundary layer is in a state of dynamical equilibrium.

### 3.2 Wall Model for Laminar Boundary Layers

As mentioned in a previous section, one of the remaining challenges in WMLES simulations is that of external flows with high Reynolds numbers. In such cases, the laminar boundary layer developing near the body leading edge is very thin, and the grid resolution required to resolve such thin region leads to a computational cost that is prohibitively high.

In this work, we propose a modeling strategy for laminar boundary layers in external flows in order to alleviate the resolution requirements needed to resolve this portion of the boundary layer in high Reynolds number flows. As such, the model presented herein seeks to calculate a wall-shear stress for boundary condition imposition, and it is argued that this condition – with the no-transpiration condition at the wall – is sufficient to recover the skin friction and pressure coefficients along the wall. This section describes the reasoning behind the model and presents its formulation, whereas the next section contains an assessment of the feasibility of the model in the aforementioned context.

The basic underlying assumption of our model is that the dynamics of the boundary layer along the wall may be given according to locally self-similar solutions. More specifically, it is assumed that at each point along the wall-tangent direction, there exists a similarity solution from the general Falkner-Skan family satisfying the boundary layer dynamics. Hence, at each point along this direction, we solve for a local similarity solution given by

$$\frac{d^3 f}{d\varepsilon^3} + \alpha f \frac{d^2 f}{d\varepsilon^2} + \beta \left[ 1 - \left( \frac{df}{d\varepsilon} \right)^2 \right] = 0 \quad (7)$$

with the boundary conditions

$$\varepsilon = 0 : \quad f = 0, \quad (8a)$$

$$\frac{df}{d\varepsilon} = 0, \quad (8b)$$

$$\varepsilon \rightarrow \infty : \quad \frac{df}{d\varepsilon} = 1, \quad (8c)$$

where  $\alpha$  and  $\beta$  are constant parameters, and  $\varepsilon$  is the similarity variable, written as

$$\varepsilon = \frac{y}{\lambda(x_s)}$$

with  $\lambda(x_s)$  a function to be defined, and  $x_s$  the distance along the surface.

In the above ordinary differential equation, the function  $f(\varepsilon)$  defines the velocity profile within the boundary layer through its first derivative,

$$\frac{df}{d\varepsilon} = \frac{u}{U_e}, \quad (9)$$

where  $u$  is the velocity within the boundary layer in the  $x_s$  direction, and  $U_e$  is the outer flow velocity, that is, the velocity at the edge of the boundary layer (Currie, 2012), which is assumed to be a function of  $x_s$  only. In boundary layer theory, this is the velocity that would be obtained for the solution in the limit of infinite Reynolds number, represented by the Euler equations.

The constant parameters  $\alpha$  and  $\beta$  in Eq. (7) may be written as

$$\frac{\lambda}{\nu} \frac{d}{dx_s} (U_e \lambda) = \alpha, \quad (10a)$$

$$\frac{\lambda^2}{\nu} \frac{dU_e}{dx_s} = \beta, \quad (10b)$$

where  $\nu$  is the kinematic viscosity. Thus, it can be seen that these two parameters define both the outer flow velocity,  $U_e$ , and the function  $\lambda(x_s)$ . Therefore, they completely define the problem to be solved. If we set  $\alpha = 1$ , then, the

corresponding similarity variable is

$$\varepsilon = y \sqrt{\frac{1}{2 - \beta} \frac{U_e}{\nu x_s}}, \quad (11)$$

and the outer flow velocity is

$$U_e(x_s) = c x_s^{\frac{\beta}{2-\beta}}, \quad (12)$$

which may be identified as the velocity of a potential flow over a wedge of half angle  $\pi\beta/2$  (Currie, 2012), as illustrated in Fig. 2.

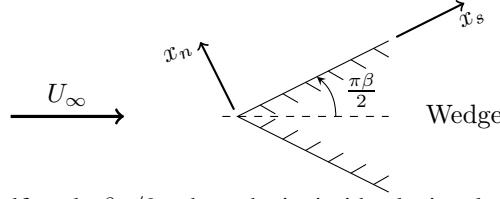


Figure 2: Flow over a wedge of half angle  $\beta\pi/2$ , where the inviscid velocity along the surface is given by Eq. (12).

In the solution process of Eq. (7), we seek a value of  $d^2 f/d\varepsilon^2$  at  $\varepsilon = 0$  that satisfies the boundary condition at  $\varepsilon \rightarrow \infty$ , Eq. (8c). This value is then used to calculate the wall-shear stress, which, for  $\alpha = 1$ , may be written as

$$\tau_w = \mu \sqrt{\frac{1}{2 - \beta} \frac{U_e^3}{\nu x_s} \frac{d^2 f}{d\varepsilon^2}} \Big|_{\varepsilon=0}, \quad (13)$$

where the definitions in Eqs. (9) and (11) are used to arrive at this final form. This wall-shear stress is subsequently used to impose the boundary condition at the wall.

Following the wall-modeling procedure described in the previous section, the outer flow velocity,  $U_e$ , appearing in the equation for the wall-shear stress above, is taken from the solution farther away from the wall, at the wall-model height,  $h_{wm}$ . It is then left to determine the parameter  $\beta$  defining the problem to be solved in Eq. (7), thus obtaining the value of  $d^2 f/d\varepsilon^2$  at  $\varepsilon = 0$ .

In order to determine the constant parameter  $\beta$ , we remind that the basic assumption of the model is that the boundary layer dynamics locally satisfies a solution of Eq. (7). As illustrated in Fig. 2, for  $\alpha = 1$ , the problem represented in Eq. (7) is that of the flow over a wedge. Thus, we assume that at each location along the body surface, the dynamics of the fluid particles are similar to those in the flow over a wedge with a half angle related to the geometric angle between the surface wall-tangent and the streamwise directions. With these assumptions, we define  $\beta$  as

$$\beta = \kappa - |\kappa| \left[ 1 - \chi \left( \frac{x}{c}, Re_c \right) \right] \quad (14)$$

where  $\kappa$  is defined such that  $\pi\kappa/2$  is the geometric angle between the wall-tangent and streamwise directions, as illustrated in Fig. 3, and, hence, may be computed as

$$\kappa = \frac{2}{\pi} \cos^{-1} (\hat{\mathbf{t}} \cdot \hat{\mathbf{s}}), \quad (15)$$

with  $\hat{\mathbf{t}}$  as the unit wall-tangent vector, and  $\hat{\mathbf{s}}$  a unit vector in the streamwise direction.

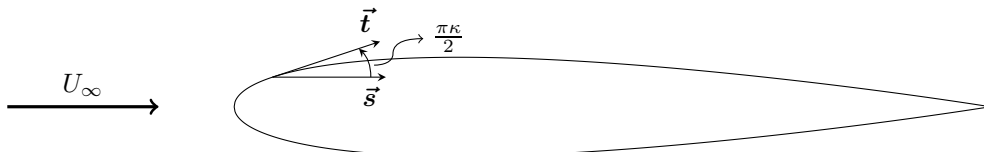


Figure 3: Definition of the geometry-related parameter  $\kappa$ , illustrated for a NACA 0012 airfoil surface.

In Eq. (14),  $\chi$  is a correction function used to adjust the angle  $\kappa$  obtained solely from geometric considerations. This correction is justified on physical grounds. If  $\beta = \kappa$  is used directly, the solution obtained from Eq. (7) is that of a flow that accelerates as much as the inviscid flow over a wedge of half angle  $\pi\kappa/2$ . In this case, the velocity gradient within the boundary layer must be higher than that obtained for a viscous flow over the same wedge and, consequently,

the computed wall-shear stress is overpredicted. The boundary layer is actually a dissipation of this gradient through viscosity, thus reducing the wall-shear stress when compared to the inviscid flow. Therefore, since  $d^2 f/d\varepsilon^2$  is directly proportional to the constant parameter defining the problem (Schlichting and Gersten, 2000), a reduction in the wall-shear stress as computed from Eq. (13) is achieved by decreasing the geometric angle  $\kappa$  in the definition of the parameter  $\beta$ .

Another way to justify this angle correction is to see the practical effect of the boundary layer as an obstruction for the flow field, acting to decrease the acceleration along the wedge. This same decreased acceleration may be obtained for the flow in a wedge with a lower half angle. Since the reasoning above applies regardless of whether  $\kappa$  is positive or negative, the adjustment is written in terms of  $|\kappa|$ .

From the rationale above, which accounts for the effects of the viscous boundary layer in the definition of the parameter  $\beta$ , it is intuitive that the correction function in Eq. (14) must be related to a Reynolds number and a characteristic length along the surface. Viscous effects become less pronounced the higher the Reynolds number, while the boundary layer grows thicker the further downstream along the surface. Since this work deals with flows around airfoils, we choose the chord Reynolds number,  $Re_c$ , and the downstream distance relative to the chord,  $x/c$ , when defining the correction function, and write it as

$$\chi\left(\frac{x}{c}, Re_c\right) = \frac{1 - \left(\sqrt{x/c}\right) e^{-A Re_c}}{1 + e^{-A Re_c}} \quad (16)$$

where  $A$  is a coefficient, and the chord Reynolds number is given by

$$Re_c = \frac{U_\infty c}{\nu},$$

with  $U_\infty$  the free-stream velocity magnitude. Note that  $x$  in the equation above is the distance in the streamwise direction, as opposed to the distance along the surface,  $x_s$ , used in the boundary layer equations.

The function in Eq. (16) has the following desired property,

$$Re_c \rightarrow \infty, \quad \chi \rightarrow 1,$$

that is, in the limit of infinite Reynolds number, no adjustment is made to the geometric angle  $\kappa$ , and the solution obtained by solving Eq. (7) refers to that of a flow accelerating as much as the inviscid flow over a wedge of half angle  $\kappa\pi/2$ , as desired. In addition, we have that

$$Re_c \rightarrow -\infty, \quad \chi \rightarrow -\sqrt{x/c},$$

and, although the above limit is not physically possible, this property means that, for a given chord Reynolds number, as  $\sqrt{x/c}$  grows larger, and hence the boundary layer thickens, the correction function  $\chi$  decreases, such that the adjustment in Eq. (14) is more pronounced.

The coefficient  $A$  is a free constant parameter to fine tune the angle correction. Preliminary parametric studies indicate that a sufficiently good value for this parameter is  $A = 2.63 \times 10^{-5}$ , and this is used throughout this work. Figure 4 shows the behavior of the correction function  $\chi$  for increasing chord Reynolds number and multiple  $x/c$  locations.

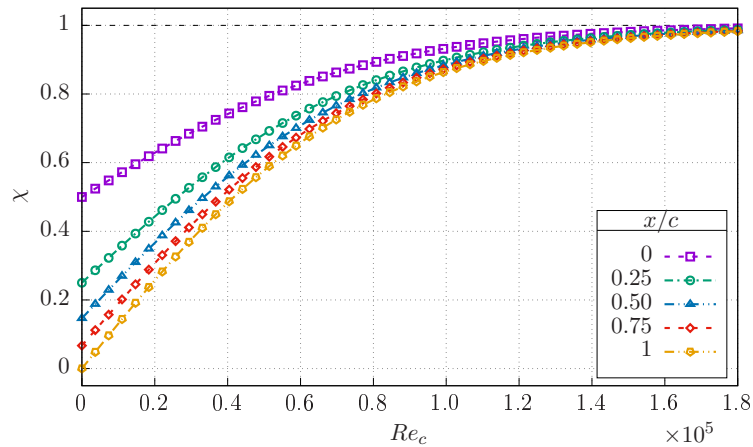


Figure 4: Correction function  $\chi$  as a function of the chord Reynolds number,  $Re_c$ , for multiple dimensionless streamwise locations,  $x/c$ .

After the definition of the parameter  $\beta$  for each location along the surface, Eq. (7) is solved using the iterative procedure described in Zhang and Chen (2009). The method employs a free boundary formulation, and uses a shooting method to transform the initial boundary-value problem into a set of initial-value problems, which are solved using standard Runge-Kutta methods. The solution using this iterative method directly outputs the quantity of interest  $d^2 f/d\varepsilon^2$  at  $\varepsilon = 0$ .

## 4. RESULTS AND DISCUSSION

This section presents the results obtained for the simulations of laminar flows around a NACA 0012 airfoil at zero angle of attack using the wall model described in Sec. 3. Since the model is only intended to be used in laminar flow regions, the test cases that constitute the validation process must exhibit relatively low Reynolds number in order to prevent transition to turbulence. At such low Reynolds numbers, it is difficult to sustain an entirely attached flow against an adverse pressure gradient, and separation of the boundary layer is likely to take place at some position downstream of the leading edge.

The validation of the wall model is done for a flow around a NACA 0012 geometry, even though separation is only absent for very low Reynolds numbers in this case. In order to keep the separation region as mild and as further away from the leading edge as possible, the current wall modeling strategy is validated primarily in a flow with a chord Reynolds number of  $Re_c = 4.5 \times 10^3$ , which remains laminar in its entirety. The Mach number for every simulation in this work is  $M_\infty \approx 0.2$ , and thus the flow is essentially incompressible. A fully resolved simulation is performed, under the same flow conditions and a sufficiently fine mesh – capable of correctly capturing the boundary layer dynamics – in a wall-resolved configuration, to provide the benchmark solution for results comparisons.

The performance of the model is assessed in terms of the predicted pressure coefficient,  $C_p$ , and skin friction coefficient,  $C_f$ , along the surface. A mesh with  $96 \times 44 \times 1$  hexahedral elements is used, where the first number indicates the elements in the direction along the surface, whereas the second indicates the elements in the wall-normal direction. The distribution of the elements along the surface is uniform, meaning that  $\Delta x_s$  is constant throughout. It should be noted that, although the flow is two-dimensional, a full, three-dimensional simulation is performed, where only a single element is generated in the spanwise direction. Figure 5 illustrates this mesh.

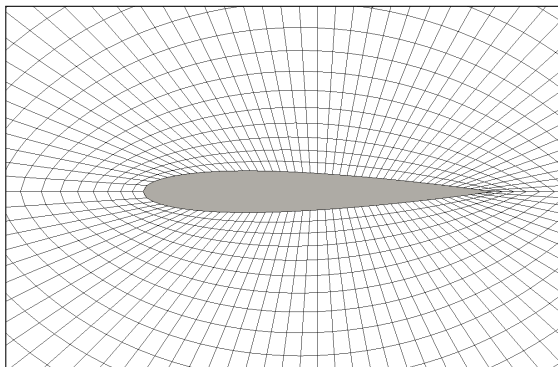


Figure 5: Two-dimensional section of the mesh employed in this work, for the region near the airfoil.

In addition, the effects of the wall-model height,  $h_{wm}$ , the main parameter of the wall-modeling procedure, are also investigated. We assume a linear growth of the exchange location where the outer flow velocity is extracted, starting from  $x/c = 0$  and increasing along the streamwise direction,  $x$ . Three different growth rates are tested, as described in Table 1 and shown in Fig. 6, where it should be noted that the wall model height,  $h_{wm}$ , is a distance from the wall in the wall-normal direction. The boundary layer edge, extracted from the fully resolved simulation, is shown for comparison.

Table 1: Shape and growth rate of the wall model height,  $h_{wm}$ , tested in the simulations.

Growth type	Growth rate	$h_{wm}(x)/c$
Linear	Low	$0.04 x/c + 0.01$
	Medium	$0.08 x/c + 0.01$
	High	$0.11 x/c + 0.01$

In the assessment of the model, the pressure and skin friction coefficients are plotted for both the upper (suction) and lower (pressure) surfaces of the airfoil, with filled symbols for the former and open symbols for the latter. As expected for a symmetric airfoil at zero angle of attack, the coefficients along the surface are exactly the same for both upper and lower surface and, hence, they are superimposed in the plots below.

The results are compared to those obtained from a fully resolved simulation, using a mesh sufficiently fine to resolve for all the viscous dynamics of the flow, with no wall modeling. In all the plots presenting the solutions, points along the lines are used only for distinguishing the different results, and are not representative of grid points.

The accuracy of the proposed wall model is first investigated using the wall model height with medium growth rate – see Fig. 6. This exchange location is chosen for the investigation because it is the one that more closely resembles the actual edge of the boundary layer. The results obtained for this simulation are shown in Fig. 7.

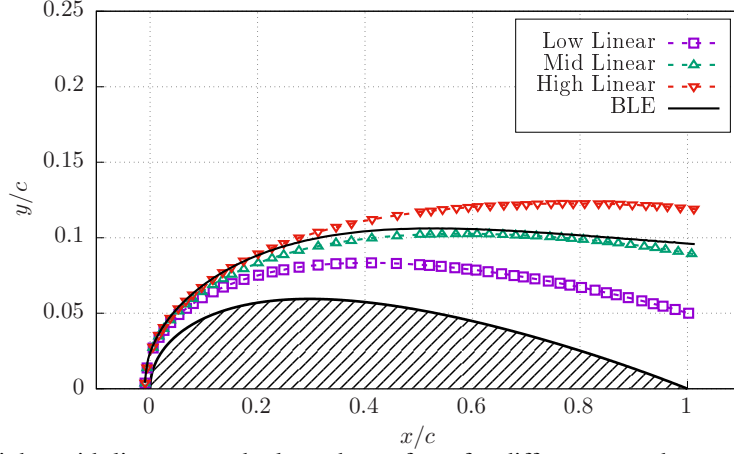


Figure 6: Wall model heights with linear growth along the surface, for different growth rates. The boundary layer edge (BLE) obtained from a fully resolved simulation is also shown.

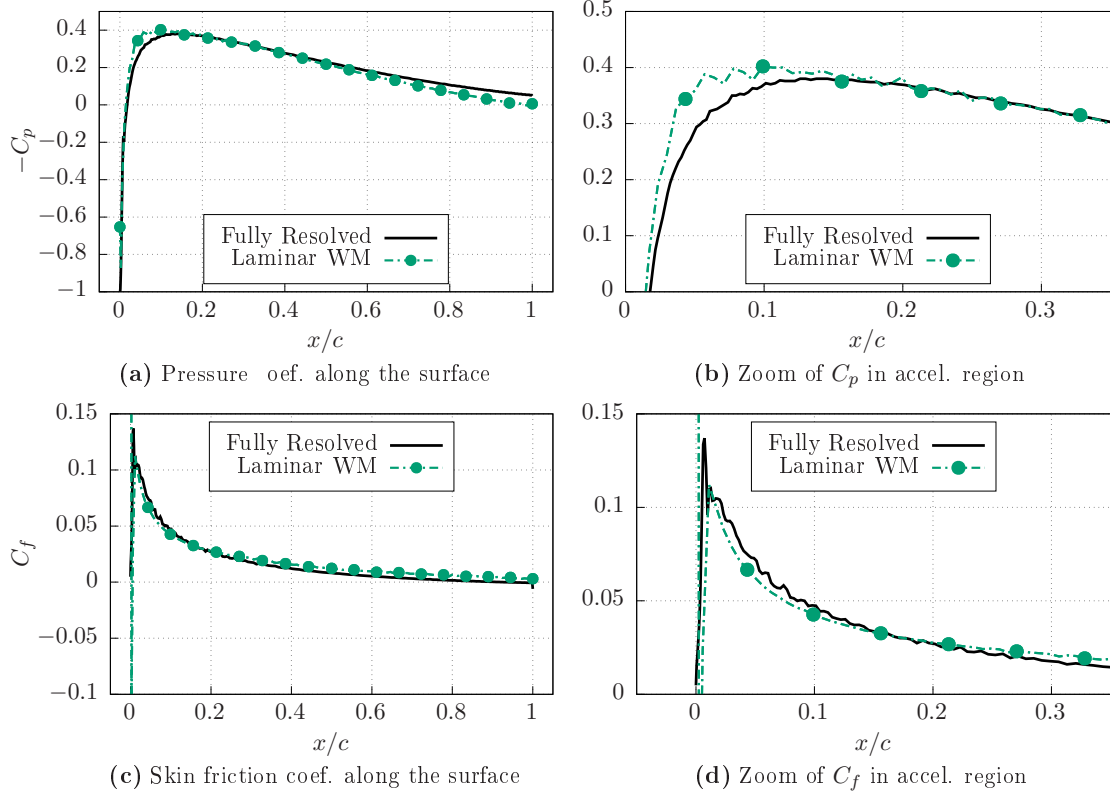


Figure 7: Solutions of pressure and skin friction coefficients for the proposed laminar wall model, using the wall model height with medium growth rate. Filled symbols: suction side; open symbols: pressure side. Symbols are superimposed.

The pressure and skin friction coefficients predicted by the model are very close to the reference solution, both qualitatively and quantitatively, despite the quite restrictive basic assumption of the model.

Near the leading edge, it is seen that the solution obtained with the wall model accelerates slightly more than the reference viscous solution, resulting in a lower pressure in this region. Moreover, the deceleration in the rear portion of the airfoil is also more pronounced, resulting in a higher pressure for the results obtained with the wall model. This is a direct consequence of imposing a lower wall-shear stress in the acceleration region, and a higher wall-shear stress in the deceleration region, when compared to the fully resolved simulation, as is evident from the results for the skin friction coefficient. This should not be seen as a flaw of the model, since the imposed wall-shear stress may be adjusted by changing the parameters of the model in the correction function  $\chi$  – cf. Eq. (14).

The behavior of the skin friction coefficient very near the leading edge, as predicted by the wall model solution, is far from the one obtained for the fully resolved simulation. It may be seen that the skin friction coefficient is very high for  $x/c \approx 0$ , followed by a narrow, negative skin friction region, from which it catches up with the expected behavior, qualitatively. From Eq. (13), defining the wall-shear stress to be imposed as the boundary condition, we see that the

leading edge,  $x/c = 0$ , is a singularity point. Thus, at this location, the wall-shear stress is ill-defined, and the wall model needs special treatment. The effect of imposing an extremely high wall-shear stress at the leading edge, when no special treatment of this location is employed, is that the flow separates, resulting in a very narrow region of reverse flow, from which it recovers shortly after, given the favorable pressure gradient.

For the solutions obtained with the wall-modeling approach, the cumulative skin friction along the surface – that is, the integrated force – is not sufficient to cause boundary layer separation. In the fully resolved simulation, however, separation occurs when the flow is approaching the trailing edge, at approximately  $x/c \approx 0.92$ . In a slightly higher Reynolds number flow,  $Re_c = 5 \times 10^3$ , separation is also present in the simulations of Swanson and Langer (2016), and it takes place at  $x/c \approx 0.8$ . It should be noted, however, that the simulations in Swanson and Langer (2016) concern compressible flows, with a Mach number of  $M_\infty = 0.5$ .

The solution for the pressure coefficient,  $C_p$ , exhibits wiggles near the leading edge. These are spurious oscillations that appear due to the fact that the mesh is too coarse to accurately represent the curvature of the airfoil geometry (Bassi and Rebay, 1997). Such spurious oscillations appear even in the solution for the fully resolved simulation, although with remarkably lower amplitude.

From the results shown in Fig. 7, the feasibility of the model is demonstrated. The discrepancies observed may be adjusted by parameter fine-tuning, and the behavior of the skin friction coefficient in the vicinity of the leading edge may be corrected by an appropriate treatment of the computed wall-shear stress at the singularity point,  $x/c = 0$ .

A very important aspect of every wall model employed in the context of wall-stress models is the effect of changes in the exchange location,  $h_{wm}$ , onto the predicted results. This parameter is usually defined in terms of the boundary layer thickness,  $\delta$ , or, similarly, the ratio  $h_{wm}/\delta$ . Since this quantity is not known prior to the simulation, a model that is insensitive to the exchange location is less restrictive in terms of the initial definition of  $h_{wm}$ .

Figure 8 shows the results obtained for the simulations using the three previously described wall model heights, with low, medium and high growth rates along the streamwise direction. These simulations are all performed in the same mesh, depicted in Fig. 5, such that any influence regarding mesh refinement or element distribution is eliminated.

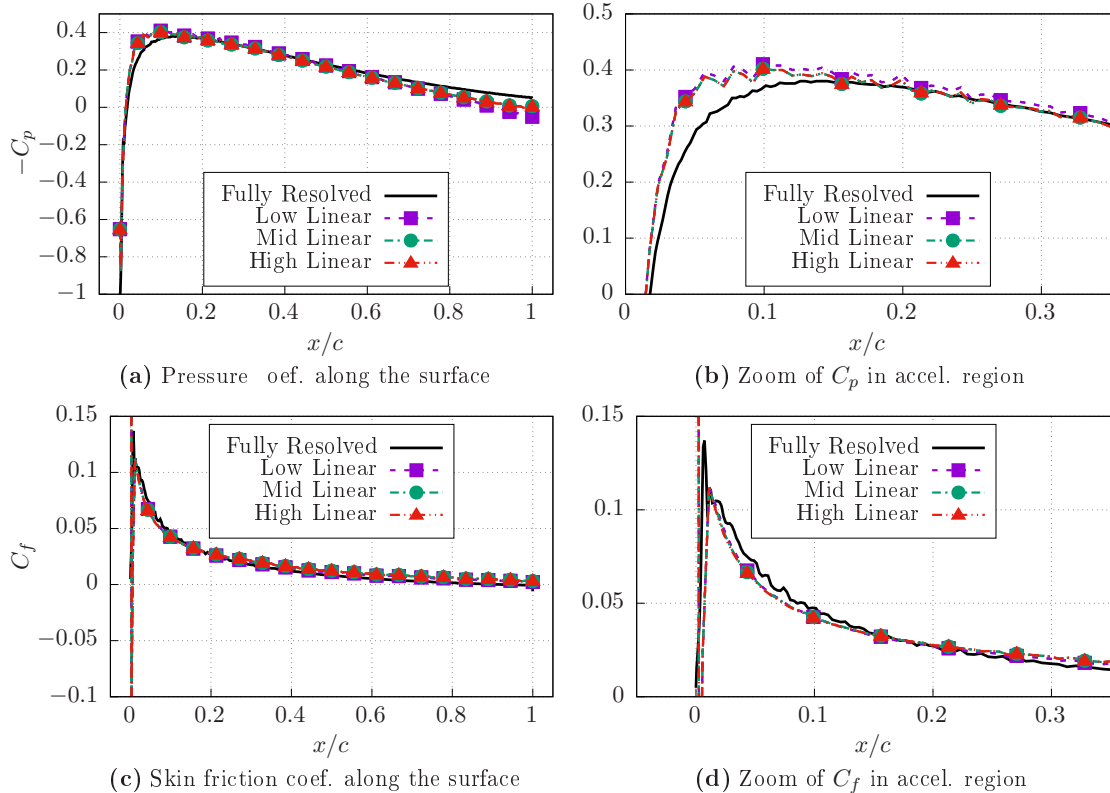


Figure 8: Solutions of pressure and skin friction coefficients for the proposed laminar wall model, using the wall model height with medium growth rate. Filled symbols: suction side; open symbols: pressure side. Symbols are superimposed.

Similar to the results shown in Fig. 7 for the medium growth rate of the wall model height, all the results shown in Fig. 8 are in very good agreement with the reference solution, especially from a qualitative point of view. When the solutions for the distinct wall model heights are compared to each other, it may be seen that only the results obtained with the smallest growth rate is distinguishable from the others. Moreover, differences are only seen for the pressure coefficient. We note that the wall model height for the lower growth rate is too close to the wall and, as a consequence, the probed velocity,  $U_e$ , is not representative of the outer flow velocity. For both medium and high growth rates, on the other hand,

the results are essentially the same, since the wall model height in these cases are farther from the wall, and more closely matches the boundary layer edge.

Since the results are very close to each other, the same behavior discussed in the previous section is observed here. The skin friction coefficient is underpredicted in the region near the leading edge, whilst being overpredicted at the rear portion of the airfoil. Consequently, the pressure is slightly lower near the leading edge due to an excess acceleration for the results using the wall modeling procedure. None of the solutions exhibit boundary layer separation near the trailing edge, however, as is expected from the behavior in the reference simulation.

Spurious oscillations appear in the solutions of the pressure coefficient for every distinct wall model height tested, as briefly discussed for the results shown in Fig. 7. This is another evidence that such wiggles are a consequence of insufficient discrete representation of the airfoil curvature, and is not related to the proposed wall model.

Another aspect of the results is that the wall-model height,  $h_{wm}$ , have very little effect on the predicted pressure coefficient. This is to be expected, since the pressure distribution at the wall is imposed from the outer flow solution and, therefore, viscous effects have little influence for fully attached flows. Nonetheless, the same behavior is observed for the predicted skin friction coefficient, where the influence of the wall model height is mild. As mentioned previously, low sensitiveness to the exchange location is an important feature of the wall model, where restrictions on the correct definition of an initial wall model height,  $h_{wm}$ , are relaxed.

## 5. CLOSING REMARKS

This work proposes a wall-modeling approach for simulations of external laminar boundary layers, based on local self-similar solutions. The wall model uses information from the numerical solution farther away from the wall, combined with local self-similar solutions of the Falkner-Skan family in order to provide a wall-shear stress that is subsequently imposed as a boundary condition. The proposed wall model is validated on simulations of an incompressible, low Reynolds number flow, with  $Re_c = 4.5 \times 10^3$  and  $M_\infty \approx 0.2$ , where the boundary layer flow remains laminar in its entirety.

The results show the feasibility of the proposed model for incompressible, low Reynolds number flows. The solutions obtained with the wall model exhibits excellent behavior for both the pressure and skin friction coefficients, following very closely the solutions obtained in a fully resolved simulation without wall modeling.

The wall model as proposed in Sec. 3., with the constant parameter  $\beta$  as defined by Eqs. (14)-(16), computes a wall-shear stress that is too low in the acceleration region, and too high in the deceleration region. Consequently, the predicted pressure distribution along the surface is too low in the acceleration region, and too high in the deceleration region. One way to adjust the computed wall-shear stress to match that obtained in a fully resolved solution is by a corresponding adjustment of the correction function,  $\chi$ , through parameter fine tuning.

An important feature of the laminar wall model is that the solutions for the pressure and skin friction coefficients are quite insensitive to the wall model height,  $h_{wm}$ . Hence, the limitations on the initial definition of the exchange location are relaxed, since locations that are not strictly matching the boundary layer edge provide reasonably accurate results.

Although spurious oscillations in the pressure distribution along the surface may be seen for every result presented in this work, we claim that such wiggles are a consequence of the mesh coarseness and its failure to accurately represent the curved geometry of the airfoil in the acceleration region.

The laminar wall model, as presented in this work, may be readily combined with a turbulent wall model in the context of wall-stress models in WMLES solutions, in order to perform a simulation of the complete developing boundary layer in external flows with reasonable computational costs for all regions and regimes of the boundary layer.

## 6. ACKNOWLEDGEMENTS

The authors acknowledge the support for the present research provided by Conselho Nacional de Desenvolvimento Científico e Tecnológico, CNPq, under the Research Grant No. 309985/2013-7. The work is also supported by the computational resources from the Center for Mathematical Sciences Applied to Industry, CeMEAI, funded by Fundação de Amparo à Pesquisa do Estado de São Paulo, FAPESP, under the Research Grant No. 2013/07375-0. The authors further acknowledge the National Laboratory for Scientific Computing (LNCC/MCTI, Brazil) for providing HPC resources of the SDumont supercomputer. This work was also granted access to the HPC resources of IDRIS under the allocation 2021-A0112A12067 made by GENCI. The first author acknowledges the financial support in the form of a doctoral scholarship from FAPESP, under the Grant No. 2018/05524-1. The third author acknowledges authorization by his employer, Embraer S.A., which has allowed his participation in the present research effort. Additional support to the fourth author under the FAPESP Research Grant No. 2013/07375-0 is also gratefully acknowledged.

## 7. REFERENCES

Bassi, F. and Rebay, S., 1997. "High-order accurate discontinuous finite element solution of the 2D Euler equations". *Journal of Computational Physics*, Vol. 138, No. 2, pp. 251–285.

- Bassi, F. and Rebay, S., 2000. “A high-order discontinuous Galerkin method for compressible turbulent flows”. In B. Cockburn, G.E. Karniadakis and C.W. Shu, eds., *Discontinuous Galerkin Methods: Theory, Computation and Applications*, Springer-Verlag, Lecture Notes in Computational Science and Engineering, pp. 77–88.
- Bose, S.T. and Park, G.I., 2018. “Wall-modeled large-eddy simulation for complex turbulent flows”. *Annual Review of Fluid Mechanics*, Vol. 50, pp. 535–561.
- Carpenter, M.H. and Kennedy, C.A., 1994. “Fourth-order 2n-storage Runge-Kutta schemes”. NASA-TM-109112, NASA Langley Research Center.
- Choi, H. and Moin, P., 2012. “Grid-point requirements for large eddy simulation: Chapman’s estimates revisited”. *Physics of Fluids*, Vol. 24, No. 1, p. 011702.
- Currie, I.G., 2012. *Fundamental Mechanics of Fluids*. CRC Press, Boca Raton, 4th edition.
- Deardorff, J.W., 1970. “A numerical study of three-dimensional turbulent channel flow at large reynolds numbers”. *Journal of Fluid Mechanics*, Vol. 41, No. 2, pp. 453–480.
- Gassner, G.J., Winters, A.R. and Kopriva, D.A., 2016. “Split form nodal discontinuous Galerkin schemes with summation-by-parts property for the compressible Euler equations”. *Journal of Computational Physics*, Vol. 327, pp. 39–66.
- Hindenlang, F., Gassner, G.J., Altmann, C., Beck, A., Staudenmaier, M. and Munz, C.D., 2012. “Explicit discontinuous Galerkin methods for unsteady problems”. *Computers and Fluids*, Vol. 61, pp. 86–93.
- Hoyas, S. and Jiménez, J., 2006. “Scaling of the velocity fluctuations in turbulent channels up to  $Re_\tau = 2003$ ”. *Physics of Fluids*, Vol. 18, No. 1, p. 011702.
- Krais, N., Beck, A., Bolemann, T., Frank, H., Flad, D., Gassner, G., Hindenlang, F., Hoffmann, M., Kuhn, T., Sonntag, M. and Munz, C.D., 2021. “FLEXI: A high order discontinuous galerkin framework for hyperbolic–parabolic conservation laws”. *Computers & Mathematics with Applications*, Vol. 81, No. 1, pp. 186–219. doi:<https://doi.org/10.1016/j.camwa.2020.05.004>.
- Larsson, J., Kawai, S., Bodart, J. and Bermejo-Moreno, J., 2016. “Large eddy simulation with modeled wall-stress: Recent progress and future directions”. *Mechanical Engineering Reviews*, Bulletin of the JSME, Vol. 3, No. 1, pp. 15–00418.
- Piomelli, U. and Balaras, E., 2002. “Wall-layer models for large-eddy simulation”. *Annual Review of Fluid Mechanics*, Vol. 34, pp. 349–374.
- Pirozzoli, S., 2011. “Numerical methods for high-speed flows”. *Annual Review of Fluid Mechanics*, Vol. 43, pp. 163–194.
- Pope, S.B., 2000. *Turbulent Flows*. Cambridge University Press. 771 p.
- Schiavo, L.A.C.A., Wolf, W.R. and Azevedo, J.L.F., 2017. “Turbulent kinetic energy budgets in wall bounded flows with pressure gradients and separation”. *Physics of Fluids*, Vol. 29, No. 11, p. 115108. doi:10.1063/1.4992793.
- Schlichting, H. and Gersten, K., 2000. *Boundary-Layer Theory*. Springer-Verlag, 8th edition.
- Schumann, U., 1975. “Subgrid scale model for finite difference simulations of turbulent flows in plane channels and annuli”. *Journal of Computational Physics*, Vol. 18, No. 4, pp. 376–404.
- Slotnick, J., Khodadoust, A., Alonso, J., Darmofal, D., Gropp, W., Lurie, E. and Mavriplis, D., 2014. “CFD Vision 2030 study: A path to revolutionary computational aerosciences”. NASA/CR-2014-218178, NASA. <https://ntrs.nasa.gov/citations/20140003093>.
- Spalart, P.R., 2009. “Detached-eddy simulation”. *Annual Review of Fluid Mechanics*, Vol. 41, No. 1, pp. 181–202. doi:10.1146/annurev.fluid.010908.165130.
- Swanson, R.C. and Langer, S., 2016. “Comparison of NACA 0012 laminar flow solutions: Structured and unstructured grid methods”. NASA/TM-2016-219003, NASA. <https://ntrs.nasa.gov/citations/20160003623>.
- Toro, E.F., 2009. *Riemann Solvers and Numerical Methods for Fluid Dynamics*. Springer-Verlag, 3rd edition.
- Zhang, J. and Chen, B., 2009. “An iterative method for solving the Falkner–Skan equation”. *Applied Mathematics and Computation*, Vol. 210, No. 1, pp. 215–222. ISSN 0096-3003. doi:<https://doi.org/10.1016/j.amc.2008.12.079>.

## 8. RESPONSIBILITY NOTICE

The authors are solely responsible for the printed material included in this paper.